Applied and Computational Mechanics 15 (2021) 133–152

Finite-element modeling of vocal fold self-oscillations in interaction with vocal tract: Comparison of incompressible and compressible flow model

P. Hájek[a,b,*], P. Švancara[a,c], J. Horáček[c], J. G. Švec[b]

[a] *Institute of Solid Mechanics, Mechatronics and Biomechanics, Brno University of Technology, Technická 2896/2, 616 69 Brno, Czech Republic*

[b] *Voice Research Laboratory, Department of Experimental Physics, Faculty of Science, Palacky University Olomouc, 17. listopadu 1192/12, 779 00 Olomouc, Czech Republic*

[c] *Institute of Thermomechanics of the Czech Academy of Sciences, Dolejškova 1402/5, 182 00 Prague, Czech Republic*

Received 13 January 2021; accepted 8 July 2021

Abstract

Finite-element modeling of self-sustained vocal fold oscillations during voice production has mostly considered the air as incompressible, due to numerical complexity. This study overcomes this limitation and studies the influence of air compressibility on phonatory pressures, flow and vocal fold vibratory characteristics. A two-dimensional finite-element model is used, which incorporates layered vocal fold structure, vocal fold collisions, large deformations of the vocal fold tissue, morphing the fluid mesh according to the vocal fold motion by the arbitrary Lagrangian-Eulerian approach and vocal tract model of Czech vowel [i:] based on data from magnetic resonance images. Unsteady viscous compressible or incompressible airflow is described by the Navier-Stokes equations. An explicit coupling scheme with separated solvers for structure and fluid domain was used for modeling the fluid-structure-acoustic interaction. Results of the simulations show clear differences in the glottal flow and vocal fold vibration waveforms between the incompressible and compressible fluid flow. These results provide the evidence on the existence of the coupling between the vocal tract acoustics and the glottal flow (Level 1 interactions), as well as between the vocal tract acoustics and the vocal fold vibrations (Level 2 interactions).

Keywords: simulation of phonation, fluid-structure-acoustic interaction, compressible flow, finite element method, biomechanics of voice

1. Introduction

Understanding the physiology and biomechanics of human voice production is the basis of voice and speech sciences. Voice is produced through self-sustained oscillations of the vocal folds (VFs) which are excited by air flowing from the lungs. The VF oscillations modulate the airflow and cause acoustic pressure oscillations; these propagate with the speed of sound through the cavities of the vocal tract (VT). The VT acts as a resonator with multiple resonance frequencies; those alter the primary sound generated at the VF level and provide the sound with the typical properties recognized as a human voice.

The voice production mechanisms should, in principle, involve the forward and backward fluid-structure-acoustic interaction (FSAI). Although the current mathematical models, which can handle such complex interaction, are mostly based on partial differential equations (PDEs),

*Corresponding author. Tel.: +420 541 142 871, e-mail: hajek.p@fme.vutbr.cz.
https://doi.org/10.24132/acm.2021.672

an extensive work has been done on the lumped-mass models mainly because of their understandability and low demands on hardware.

Based on the first groundbreaking models [26, 33, 57], the recent lumped-mass models are capable of capturing linear or non-linear interactions between the physical domains [75, 77], chaotic behavior of the VFs in some regimes [78, 79], bulged shape of the VFs [31, 47] or sound of the vowel [iː] [33, 46].

The PDE-based models are still using many simplifications because of their computational costs. The typical simplification is to solve interactions between two of physical domains, e.g., the fluid-structure interactions (FSIs). The FSIs have been commonly solved in many engineering applications [6, 8, 55]. In the field of voice research, the early PDE-based model that introduced the one-way FSI was that of Alipour et al. [3].

The FSI models were gradually developed to include VF self-oscillations [1, 2, 69], which turned out to correspond well with previous theoretical studies [70, 71] and found that cyclic changes of the VF profile from convergent to divergent shape play a crucial role in the fluid-structure energy exchange allowing sustained VF self-oscillations.

Later models added the VF collisions [19, 68]. Periodical flow separation during the VF oscillation allowed to observe flow behavior in glottis during oscillatory cycle. The largest pressure drop occurred between divergent shape of the VF. This phenomenon is in an agreement with the concept of the myoelastic-aerodynamic theory of phonation [14, 66, 73] and with the recent experimental and computational results [4, 19, 27, 52, 69].

To obtain information on the sound generated due to the pulsating flow produced by the oscillating VFs, fluid-acoustic interaction (FAI) needs to be taken into account [36]. Several theories, i.e. acoustic analogies, have been developed to describe the airflow-generated sound. These involve Lighthill's analogy [41, 42], Curle's analogy [18], Ffowcs Williams-Hawkings (FWH) method [25] or acoustic perturbation equations (APE) [22].

Many authors created new models of phonation with a prescribed movement of the VF and the acoustic analogy or APE. They showed that the dominant acoustic source is the sound generated by the flow through the glottis [9, 34, 58, 85] and the prescribed (driven kinematic) VF movement is reasonable simplification resulting in lower computational costs [24, 50, 51, 63, 87]. Yet Alipour et al. upgraded their model [2, 4] with the self-oscillating VFs and found that the distributions along the centerline axis in this model were similar as in [19, 27, 52, 69] and the presented formants of the vowels [aː] and [iː] were in good correspondence to those observed in humans. The self-oscillating model of Link et al. [43] demonstrated the possibilities of the FSAI.

The above-mentioned incompressible glottal flow models with the acoustic analogies offer an indirect way to acquire acoustic pressure from the behavior of an incompressible flow. The direct way requires calculation of the acoustic pressures using the compressible Navier-Stokes equations (NSEs). Acoustic pressures are then inherent part of such a solution. This attitude is, however, by far the most computationally expensive, especially for low Mach number flows (below 0.3), due to a disproportion in flow and sound velocities [6, 9, 17, 43].

Overcoming these problems, Zhang et al. [84] used the compressible NSEs to calculate airflow and sound generated through prescribed motion of the glottis and compared the results to those from the FWH method. The results were in a good agreement.

Shickhofer et al. [53, 54] also used compressible NSEs. Although the source signal was generated by the Rosenberg glottal pulse model [48] instead of self-oscillating VFs, they simulated five vowels on a realistic geometry. Results showed that first formants of all simulated vowels were in good agreement with measured formant frequencies. The measured sound signal was obtained during magnetic resonance (MRI) scan.

To the best of our knowledge, there has not been any study including the compressible NSEs and complete FSAI involving the self-oscillating VFs. The model presented here is based on previous studies of the authors [28, 29, 64, 65] where an finite-element (FE) model of the vocal organs during phonation of Czech vowels was developed. In this study, new two-dimensional (2D) FE models of flow-induced oscillations of the VFs, in interaction with acoustic spaces of the VT, were constructed to enable calculations using either compressible or incompressible airflow.

Although the 2D assumption carries several simplifications, e.g., different formation of turbulence in the VT, absence of spatial vortices or no anterior-posterior modes of VF vibration, it is used here for the sake of a radical reduction of computational costs [62]. It was shown that, up to 3000 Hz, the influence of the spatial dimension of the VT is rather insignificant [80].

The aim of this study was to directly compare the effect of air compressibility on VFs oscillations using an identical FE mesh, identical boundary conditions and identical FSI formulation for compressible and incompressible airflow model. The computed quantities are compared to data found in the literature.

The description of the computational model is divided into sections concerning the geometry of the VF and VT, FE setup, the material model and parameters, the boundary conditions, and the algorithm of the FSAI implementation including the mathematical formulation of the structural and fluid domains.

2. Methods

2.1. Vocal fold and vocal tract geometry

The geometry of the VFs was based on the widely used parametric M5 shape, see Scherer et al. [52]. To take into account the layered structure of the VFs [72], four layers of the VF tissue were included in the model – epithelium, superficial layer of lamina propria (SLP), ligament (intermediate and deep layers of the lamina propria) and muscle [72, 73]. The geometry of the VT was based on data registered by the MRI during male phonation of the Czech vowel [iː] [20, 80].

2.2. Finite element model

A 2D FE model of the VF and of the VT with trachea were developed using the software package ANSYS® Academic Research Mechanical, Release 15.0. The FE models of the four-layered tissue of the VFs and of the airways in the VT for the vowel [iː] are shown in Fig. 1. This figure shows also the details of the fluid mesh in the glottal region (marked by the red rectangle) which contains 12 fluid elements over the glottal width. The dimensions of the models are specified in Table 1. The FE model consists of 5 350 linear 3-node and 4-node structural elements, 10 747 linear 4-node fluid elements and 2×24 contact elements, which ensure a symmetric contact pair, i.e., the VF collisions. The structural and contact elements have two degrees of freedom (DOF) in each node (displacement in x and y directions) and fluid elements have three DOFs for incompressible flow (velocities in x and y directions and pressure) and four DOFs for compressible flow (velocities in x and y directions, pressure and temperature).

In comparison with [28, 64, 65], the fluid mesh was refined to capture smaller eddies in the airflow. The size of the fluid element in the y direction between the VFs was 0.025 mm typically. This size was gradually increasing to approximately 5 mm near the lips and near the entrance to the trachea. Taking into account the condition of 10 nodes (or 9 linear elements) per acoustic

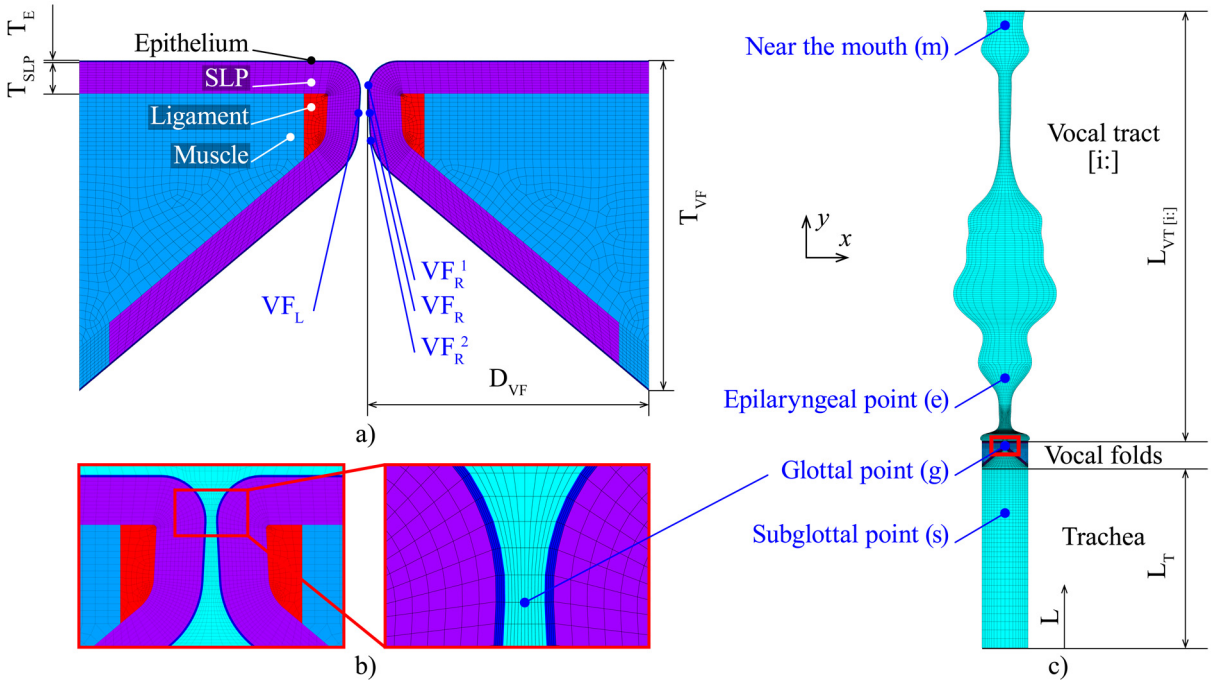

Fig. 1. a) The four-layered FE model of the VFs; b) details of the FE mesh in the glottal region; c) the 2D FE model of Czech vowel [i:]. The blue points marked on the VF contact surfaces, in the trachea and in the VT are the evaluating points, i.e., points, where the simulated time signals were observed. The indicated spatial parameters are numerically specified in Table 1. The L coordinate shown in c) denotes the length of the whole FE model

Table 1. Dimensions of the model

Epithelium thickness T_E [mm]	0.05	Inferosuperior thickness T_{VF} [mm]	11.00
SLP thickness T_{SLP} [mm]	1.00	Trachea length L_T [mm]	74.00
Mediolateral depth D_{VF} [mm]	9.00	Length of VT for [i:] $L_{VT[i:]}$ [mm]	175.61

wavelength [7], the fluid mesh can handle frequencies up to 7 844 Hz. This limit is reasonable since the time step value lowers the maximal frequency range to 5 000 Hz due to sampling reasons. Majority of the acoustic energy contained in the spectrum of human voice is located below 5 000 Hz [12, 59].

2.3. *Material used for the model*

Each layer of the VFs was considered to be a homogeneous isotropic linear elastic material with properties derived from [35, 73] and tuned in [28, 29, 64, 65], see Table 2. Properties of the dry air were set to the parameters known for the ideal gas of 36 °C [6], see Table 3. The speed of sound c_{air} $[\mathrm{m}\cdot\mathrm{s}^{-1}]$, as a function of the equation of state and its absolute temperature, was acquired from the well known equation

$$c_{air} = \sqrt{\kappa R T} \approx 331.6 \cdot \sqrt{1 + \frac{t}{273.1}}, \tag{1}$$

where κ is the heat capacity ratio given in Table 3, R is the universal gas constant with the value of 287.05 $\mathrm{J}\cdot\mathrm{kg}^{-1}\cdot\mathrm{K}^{-1}$, T is the air temperature in [K] and t is the air temperature in [°C].

Table 2. Material properties of the VFs

VF layer:	Young's modulus E [Pa]	Poisson's ratio μ [–]	Density ρ_s [kg · m^{-3}]
Epithelium	25 000	0.49	1040
SLP	2 000	0.49	1040
Ligament	8 000	0.49	1040
Muscle	65 000	0.40	1040

Table 3. Material properties of air

Air:	Speed of sound c_{air} [m · s^{-1}]	Dynamic viscosity η [Pa · s]	Density ρ_f [kg · m^{-3}]	Heat capacity ratio κ [–]
36 °C	353	$1.813\,51 \cdot 10^{-5}$	1.205	1.4

In order to insert the damping of the VF layers to the ANSYS® transient analysis (see Section 2.5), proportional (Rayleigh) damping coefficients α (mass-proportional damping) and β (stiffness-proportional damping) were used. These two coefficients were acquired using the modified formulas from [23]

$$\alpha = 2\pi f_1 \cdot (b_{p1} - \pi f_1 \beta), \tag{2}$$

$$\beta = \frac{b_{p2} - \frac{f_1}{f_2} b_{p1}}{\pi \cdot \left(f_2 - \frac{f_1^2}{f_2} \right)}. \tag{3}$$

The damping coefficients for the SLP layer required as an input a pair of chosen damping ratios $b_{p1} = 0.20$ and $b_{p2} = 0.30$ [15, 37, 67] and a pair of natural frequencies $f_1 = 70.65$ Hz and $f_2 = 142.54$ Hz of the undamped VF computed by modal analysis in the ANSYS®. Thus, the damping of the SLP layer resulted in $\alpha = 60.377\,6$ s^{-1} and $\beta = 0.000\,6$ s.

The damping of the other layers of the VFs was set to $\alpha = 116.527\,9$ s^{-1} and $\beta = 0.000\,4$ s, which correspond to damping ratios $b_{p1} = b_{p2} = 0.2$ at the above mentioned natural frequencies f_1 and f_2.

2.4. Boundary conditions

Boundary conditions and loading were applied in the same manner in both the FE models. The entrance to the trachea was excited by a constant lung pressure $p_L = 270$ Pa (over the considered atmospheric pressure of the 101 350 Pa) as the only driving parameter. This lung pressure is at the lower end of the physiological values observed in humans [10]. Such a low value of the p_L was chosen to avoid excessive fluid mesh distortion in the glottal region observed at higher lung pressures.

Zero pressure was applied at the end of the VT to simulate open lips. Radiation to an open space was not considered in this study, similarly as in other studies [19, 43, 60, 62, 83, 86, 87]. The PML layer of elements used in some models [24, 63] could not be applied here because the PML layer is designated for acoustical elements rather than the elements for fluid flow simulations.

Rigid walls of the VT and trachea were set to be totally reflective with no-slip condition for the fluid flow. The VFs were clamped at the lateral ends.

2.5. Fluid-structure-acoustic interaction algorithm

The FE model of the FSAI was solved in a time domain using a transient analysis with the time step of $1 \cdot 10^{-4}$ s. The structural model (VFs) was described by a momentum equation [6, 13, 21]

$$\rho_s \frac{\partial^2 \mathbf{u_s}}{\partial t^2} - \nabla \boldsymbol{\tau}_\mathbf{s} = \mathbf{f_s}, \tag{4}$$

where ρ_s is the density of the structural model, $\mathbf{u_s}$ are the unknown displacements, $\boldsymbol{\tau}_\mathbf{s}$ is the Cauchy stress tensor and $\mathbf{f_s}$ is the structural load vector. The structural model was coded in ANSYS® Parametric Design Language (APDL) and included large deformations and VF collisions. The generalized Hilber-Hughes-Taylor time integration method (HHT-α method) was used for the time integration of the momentum equation [6]. For this purpose, the momentum equation (4) had to be transformed to a weak formulation and discretized by the FE method, which led to a system of equations

$$\mathbf{M}\ddot{\mathbf{u}}(t) + \mathbf{C}\dot{\mathbf{u}}(t) + \mathbf{K}\mathbf{u}(t) = \mathbf{F_s}(t)\,, \tag{5}$$

where $\mathbf{M}$, $\mathbf{C}$, and $\mathbf{K}$ are the structural mass, damping and stiffness matrices, $\ddot{\mathbf{u}}(t)$ is the nodal acceleration vector, $\dot{\mathbf{u}}(t)$ is the nodal velocity vector, $\mathbf{u}(t)$ is the nodal displacement vector and $\mathbf{F_s}(t)$ is the applied load vector.

The airflow model in the trachea and the VT was developed in the ANSYS® FLOTRAN™ code. The governing equations consist of the continuity equation, the unsteady viscous compressible NSEs and the energy equation for the adiabatic process.

All of the equations except the continuity equation, which will be discussed later, could be written in a unified form as follows [5, 11, 82]

$$\frac{\partial}{\partial t}(\rho_f v_x) + \frac{\partial}{\partial x}(\rho_f v_x^2) + \frac{\partial}{\partial y}(\rho_f v_x v_y) = \frac{\partial}{\partial x}\left(\eta \frac{\partial v_x}{\partial x}\right) + \frac{\partial}{\partial y}\left(\eta \frac{\partial v_x}{\partial y}\right) + \rho_f g_x - \frac{\partial p}{\partial x} + R_x, \tag{6a}$$

$$\frac{\partial}{\partial t}(\rho_f v_y) + \frac{\partial}{\partial x}(\rho_f v_x v_y) + \frac{\partial}{\partial y}(\rho_f v_y^2) = \frac{\partial}{\partial x}\left(\eta \frac{\partial v_y}{\partial x}\right) + \frac{\partial}{\partial y}\left(\eta \frac{\partial v_y}{\partial y}\right) + \rho_f g_y - \frac{\partial p}{\partial y} + R_y, \tag{6b}$$

$$\frac{\partial}{\partial t}(\rho_f C_p T) + \frac{\partial}{\partial x}(\rho_f v_x C_p T) + \frac{\partial}{\partial y}(\rho_f v_y C_p T) = \frac{\partial}{\partial x}\left(K \frac{\partial T}{\partial x}\right) + \frac{\partial}{\partial y}\left(K \frac{\partial T}{\partial y}\right) + Q_v + E_k + W_v + \Phi + \frac{\partial p}{\partial t}. \tag{6c}$$

The solved variables are: v_x – fluid velocity in x direction, v_y – fluid velocity in y direction, T – temperature and p – pressure. The coefficients C_p, K, Q_v, g_x and g_y stand for the specific heat of $1\,004\ \mathrm{J \cdot kg^{-1} \cdot K^{-1}}$, the thermal conductivity of $2.699\,5 \cdot 10^{-2}\ \mathrm{W \cdot m^{-1} \cdot K^{-1}}$, the volumetric heat source and the gravity acceleration components in x and y directions, respectively. The distributed resistances R_x and R_y represent any source term one may wish to add.

The kinetic energy E_k, the viscous work term W_v and the viscous dissipation term Φ can be expressed as

$$E_k = -\frac{\partial}{\partial x}\left\{\frac{K}{C_p}\frac{\partial}{\partial x}\left[\frac{1}{2}\left(v_x^2+v_y^2\right)\right]\right\} - \frac{\partial}{\partial y}\left\{\frac{K}{C_p}\frac{\partial}{\partial y}\left[\frac{1}{2}\left(v_x^2+v_y^2\right)\right]\right\}, \tag{7a}$$

$$W_v = v_j\eta\left(\frac{\partial}{\partial x_i}\frac{\partial v_j}{\partial x_i} + \frac{\partial}{\partial x_k}\frac{\partial v_k}{\partial x_j}\right), \tag{7b}$$

$$\Phi = \eta\left(\frac{\partial v_i}{\partial x_k} + \frac{\partial v_k}{\partial x_i}\right)\frac{\partial v_i}{\partial x_k}, \tag{7c}$$

where the latter two terms are written in the Einstein summation convention.

The complete set of the governing equations, except the continuity equation, is closed by the thermodynamic state relations

$$\frac{\partial \rho_f}{\partial p} = \frac{1}{RT}, \tag{8a}$$

$$T = T_0 - \frac{1}{2}\frac{v_x^2+v_y^2}{C_p}, \tag{8b}$$

where R is the universal gas constant given in Section 2.3 and T_0 is the total (stagnation) temperature of 309 K.

The NSEs and the energy equation (6) were discretized by the Galerkin method of weighted residuals [5] which results in solution of the system of equations

$$\left(\mathbf{A}_\mathbf{e}^{\mathbf{Trans}} + \mathbf{A}_\mathbf{e}^{\mathbf{Advect}} + \mathbf{A}_\mathbf{e}^{\mathbf{Diff}}\right)\cdot\boldsymbol{\alpha}_e(t) = \mathbf{S}_\mathbf{e}^{\alpha}(t), \tag{9}$$

where $\mathbf{A}_\mathbf{e}^{\mathbf{Trans}}$, $\mathbf{A}_\mathbf{e}^{\mathbf{Advect}}$ and $\mathbf{A}_\mathbf{e}^{\mathbf{Diff}}$ are the element matrix contributions from the transient, advective and diffusion terms, $\boldsymbol{\alpha_e}(t)$ is an element vector of the considered variables, and $\mathbf{S}_\mathbf{e}^{\alpha}(t)$ is the element vector of the source terms. The Newmark method was used for time integration. The element integrals of the transient term $\mathbf{A}_\mathbf{e}^{\mathbf{Trans}}$ were formed by the pure Galerkin method. The advection term $\mathbf{A}_\mathbf{e}^{\mathbf{Advect}}$ was handled through the streamline upwind/Petrov-Galerkin approach (SUPG), and the diffusion term $\mathbf{A}_\mathbf{e}^{\mathbf{Diff}}$ was integrated by parts over the fluid domain [5].

The flow model included the solution of pressures. From the state equations (8) and the continuity equation

$$\frac{\partial \rho_f}{\partial t} + \frac{\partial(\rho_f v_x)}{\partial x} + \frac{\partial(\rho_f v_y)}{\partial y} = 0, \tag{10}$$

the pressure correction equation is derived which enables to use the segregated velocity-pressure solution. This nonlinear solution procedure belongs to a class of semi-implicit method for pressure linked equations (SIMPLE) handled by ANSYS® FLOTRAN™ [5,82]. The enhanced SIMPLEN algorithm was used in the case of compressible fluid and the SIMPLEF algorithm was used in the case of incompressible fluid [5].

The incompressible fluid assumption breaks the linkage between the continuity equation and NSEs on one hand and the energy equation on the other hand [82]. Omitting density variations also simplifies the continuity equation and the NSEs. The energy equation is not solved in such a case and therefore one DOF (the temperature T) is spared, which leads to shorter solution times. The sufficiently high bulk modulus of 10^{15} Pa was used in the incompressible state equation (8a) instead of the term RT [5].

Each DOF (independently on the compressibility) was solved in a sequential order. Each equation was solved with intermediate values of the surrounding DOFs. The solution of all the equations in turn and subsequent update of the values is referred to as global iteration [5]. Only a few global iterations are usually sufficient to achieve default convergence criteria (normalized rate of change of each DOF over the solved domain) of the all DOFs: $1 \cdot 10^{-12}$ for pressure and temperature and $1 \cdot 10^{-5}$ for velocities.

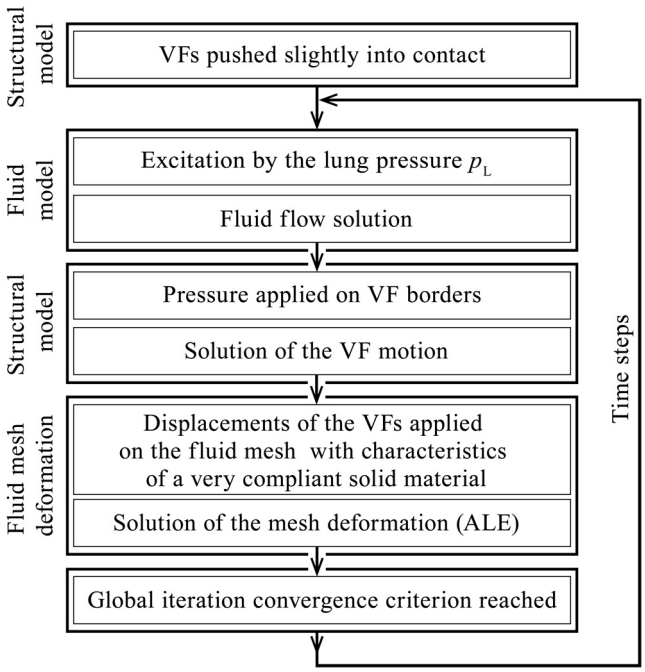

Fig. 2. The FSAI algorithm

The FSAI algorithm is schematically described in Fig. 2. Before initiation of the FSAI computation, the VFs were located 0.2 mm from each other. Then, they were slightly adducted and put into contact. This was realized as a static analysis (the solution of deformation) of the structural model. The VFs were pushed together by a prescribed displacement 0.3 mm at both lateral ends.

Afterwards, the FSAI were solved using explicit coupling scheme with separated solvers for the structural and fluid model in the global iterations [5]. The results of the airflow solution were transferred as loads on the VF surface. This then allowed computing the VF motion. In the last part of the algorithm, the material of the fluid mesh was changed to a very compliant solid material which allowed morphing of the fluid mesh geometry based on the VFs displacement. The arbitrary Lagrangian–Eulerian (ALE) approach was utilized to represent moving boundaries of the fluid domain. The distance between the faces of the VFs was monitored during the solution; when it was below the defined minimal distance (0.15 mm used here), the mesh morphing was stopped at these elements and the flow velocity was set to zero. Under these conditions, the structure and fluid nodes were temporarily decoupled and were allowed to come into contact. Collision between the two VFs was modelled by a symmetric surface-to-surface contact pair of face elements solved by the augmented Lagrangian method implemented in the ANSYS® Academic Research Mechanical, Release 15.0. Coulomb friction was assumed between the contact surfaces. The default friction coefficient of 1.0 was used to achieve sticking during the glottal closed phase.

2.6. Studied output and evaluation of results

The results from the structural model were assessed from the selected nodes of the VF surface (see the evaluating points marked in Fig. 1a). Vocal fold edge waveforms were captured from the minimal width of the glottis in the medial-lateral direction in each iteration (VF^L_{min}, VF^R_{min}). Also, the vibration characteristics were evaluated from the VF^L_{min}, VF^R_{min} to capture the maximum glottal width (W_g^{max}), open quotient (OQ), closing quotient (ClQ), speed quotient (SQ) and fundamental frequency of VF vibration (f_o) [44].

The fluid results were evaluated in four points: 30 mm below (point s), 1 mm below (g), 30 mm above the upper surface of the VFs (e), and 5 mm up-stream from the lips (m), recall Fig. 1c.

Electroglottographic (EGG) signal [73] was simulated by calculating the ratio between the number of surface epithelium elements in contact and the total number of the elements (in our case 24) on medial VF surface. All 24 elements in contact produced the EGG value of 1 and none of the 24 elements produced value of 0. In order to avoid discontinuities due to density of the structural mesh, the data were subjected to a Gaussian smoothing implemented in MATLAB® R2017a.

3. Results and discussion

3.1. Influence of air compressibility on motion of the vocal folds

Fig. 3 shows typical results for displacements of the VFs in x direction during the phonation of vowel [iː] while Table 4 compares VF vibration characteristics for the compressible and incompressible flows evaluated from Fig. 3.

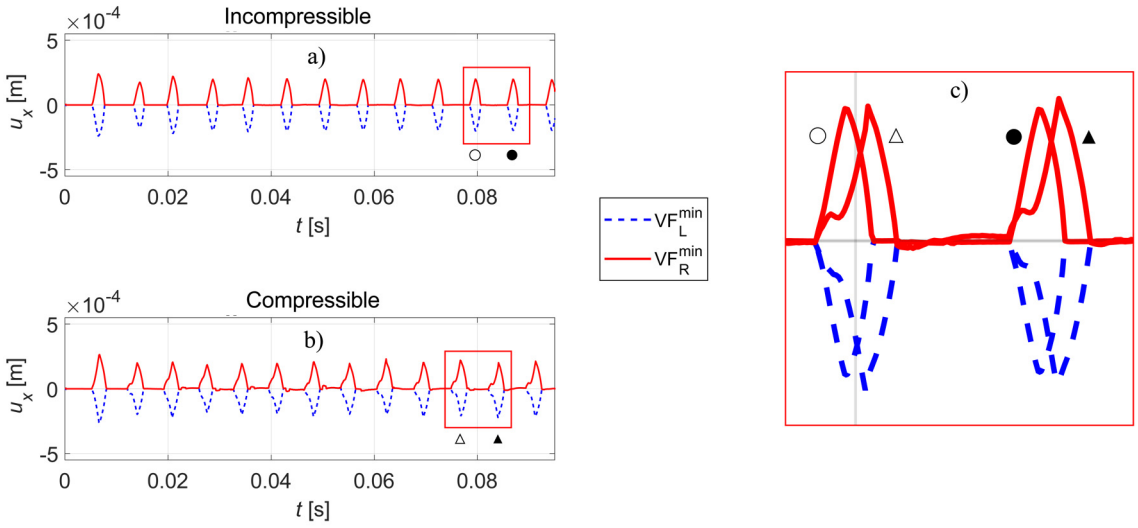

Fig. 3. Vocal fold edge waveforms in vowel [iː] for a) incompressible and b) compressible flows. Detailed comparison of two aligned periods is shown in c). Empty and filled circlets denote the chosen periods for the incompressible flow solution, and empty and filled triangles denote the chosen periods for the compressible flow solution

Table 4. Vibration characteristics of the VFs

Compressibility	W_g^{max} [mm]	OQ [–]	ClQ [–]	SQ [–]	f_o [Hz]
Off	0.39	0.28	0.13	1.10	133
On	0.43	0.42	0.15	1.82	137

The maximum glottal width W_g^{max} is 7.97% higher (0.39 mm vs. 0.43 mm) in the case of compressible fluid flow. The higher W_g^{max} results from the more compliant environment of the compressible flow compared to incompressible flow and from the structure-acoustic interaction (SAI) below the first acoustic resonance in the VT. The W_g^{max} through the both computed variants was less than 0.5 mm which is about 2–4 times less than the usual width of glottis reported in the literature [4, 72]. Such an effect is caused by the small subglottic pressure p_L considered in this study. The rather small pressure p_L influences also other quantities proportionally, more in Section 3.2.

A small peak located at the beginning of the opening phase was observed in the compressible solution, see Fig. 3c. This can be attributed to the interaction of the acoustic waves with the VF vibrations: the little peak was missing in the first period of the compressible flow when the acoustic wave was not yet fully present in the VT.

The small peak prolonged open phase and made it unsymmetrical. On that account the OQ from compressible solution falls within the range observed in human male subjects during normal phonation, where the 95% confidence interval of the OQ has been reported to be 0.36–0.76 in the middle of glottis [44], even though the low p_L used here applies rather to a soft phonation. More unsymmetrical open phase caused that SQ is higher than men's 95% confidence interval 0.32–1.44 [44] contrary to SQ from incompressible solution, which lies in that interval. Asymmetry of the open phase is also demonstrated by ClQ.

Combination of longer open phase and shorter closed phase in compressible model (visible in Fig. 3c) lead to 2.74% higher fundamental frequency f_0 (133 Hz vs. 137 Hz).

These differences show interaction between acoustics at compressible solution and other domains and therefore illustrates the importance of the SAI for the behavior of the voice source. Similar effect was published in [46], where changes in CQ and ClQ were caused dominantly by the acoustic loading.

3.2. Comparison of the simulated waveforms

Fig. 4 plots the computed waveforms of aerodynamic, vibratory, acoustic and EGG signals for both the incompressible (left) and compressible (right) airflow solution in the vowel [i:]. The compressible-incompressible differences are most apparent when comparing any of the pressure signals (Figs. 4a and 4b) or the power spectral densities (PSDs, Figs. 4m and 4n); these are largely influenced by the acoustic waves propagating in the compressible air.

The acoustic waves are apparent as oscillations in both subglottal (p_s) and epilaryngeal (p_e) pressure signals in the compressible case (Fig. 4b). The peaks occurring in the p_s and p_e in the incompressible case (Fig. 4a) are caused solely by the VF self-oscillations. In both compressible and incompressible cases, the subglottal pressure p_s oscillates around the mean value $p_L = 270$ Pa and the epilaryngeal pressure p_e oscillates around 0 Pa, as expected.

In both cases, the VFs vibrate with phase differences between the lower and upper margins. This can be observed in the displacements u_x of the two nodes VF_R^1 and VF_R^2 (Fig. 4c, d); recall Fig. 1 for location of these nodes. The glottal width W_g is wider in the case of compressible flow as shown also in Fig. 3c.

The flow velocity waveforms v_g (Figs. 4e and 4f) are similar to each other, with higher maxima in the case of the incompressible flow. Notice that the velocity maxima occur at the very end of the open phase when the glottal width becomes small. This is mainly caused by the inertance of a fluid column: the fluid flow, see Fig. 4e, leads the pressure, see Fig. 4a, in phase as in [75]. The waveform shapes are very similar to those obtained by Alipour and Scherer [4], only the v_g maximum is about two times lower in our case which is related to the four times lower p_L used here compared to [4, 72].

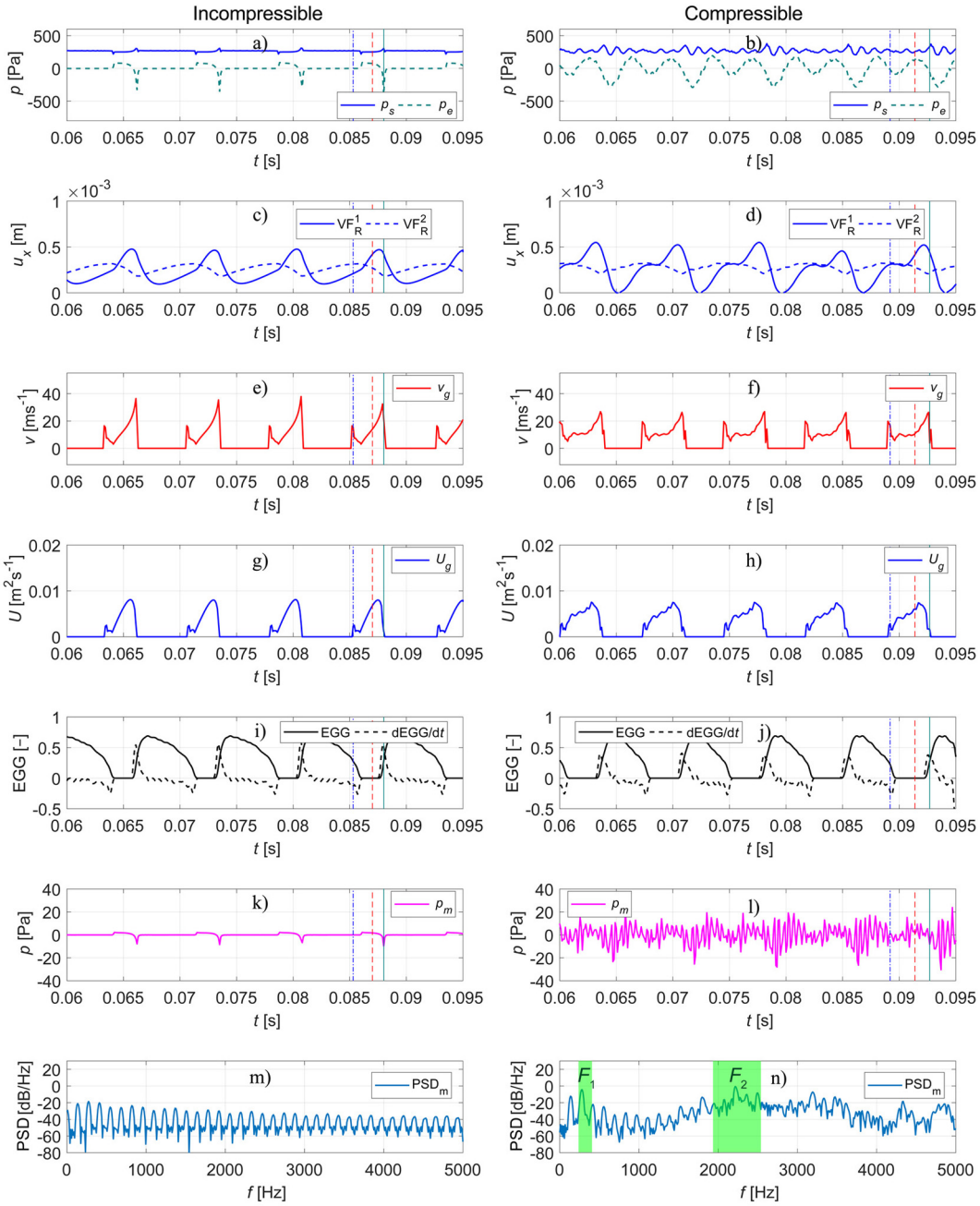

Fig. 4. Comparison of the results obtained for incompressible (left panels) and compressible flow (right panels); a), b) subglottal pressure (p_s) and epilaryngeal pressure (p_e); c), d) displacements in x direction (u_x) of the two nodes VF_R^1 and VF_R^2; e), f) flow velocity between the VFs (v_g); g), h) glottal flow (U_g) on the level of the nodes VF_R and VF_L; i), j) EGG signal and its time derivative; k), l) pressures near the mouth (p_m); m), n) the power spectral density near the mouth (PSD_m) from the p_m windowed by the Hamming window of 512 samples length. The time instances shown by the blue, red and green vertical lines in panels a)–l) approximately correspond to the phases at which the glottis takes convergent, parallel and divergent glottal shapes, respectively (see also Figs. 5 and 6)

The shape of the v_g is related to the glottal flow volume velocity U_g (Figs. 4g and 4h): zero U_g occurs during the glottal closure matching the v_g.

The simulated EGG signal confirms that the contacting phase is significantly shorter than the decontacting phase; this agrees with the observations of normal EGG waveforms in human phonations for vowel [i:] [16].

The pressures near the mouth p_m are shown in Figs. 4k and 4l. Whereas in the incompressible case (Fig. 4k) these pressure waveforms are similar to the epilaryngeal pressures p_e (recall Fig. 4a), the compressible case (Fig. 4l) reveals pressure fluctuations related to the acoustic resonances of the VT.

The power spectral densities (PSDs) of the pressures p_m are displayed in Figs. 4m and 4n. The compressible case (Fig. 4n) shows formant peaks in PSD which are well within the normal range of formant frequencies $F_1 \approx 215$–348 Hz and $F_2 \approx 1952$–2558 Hz (marked with green) reported for the Czech vowel [i:] [56]. The formant frequencies approximate the first two resonances of the VT calculated by the 2D and also 3D modal analysis in ANSYS®. In both cases, they were 318 and 1957 Hz, respectively. The boundary conditions were in accordance with the open lips and closed VFs. The simulated formants were validated previously using an experimental setup with the identical geometry of the VT made from plexiglass [32] and also by the sound signal of the same vowel [i:], which was acquired during the scan of the original geometry in MRI [80]. The simulated formants fit the measured [i:] vowel formant ranges from both [32] and [80].

No formant peaks occur for the incompressible flow (Fig. 4m), reflecting the fact that there are no acoustic waves propagating in the VT in this case.

3.3. Compressibility influence on air pressures and velocities

The flow velocities in the glottis region, together with the VF shape, are depicted in Fig. 5 for three different time instants at which the VFs take convergent, parallel and divergent cross-sectional shapes. The jet deflection of fluid flow above the VFs appears during typical oscillation period always, as shown.

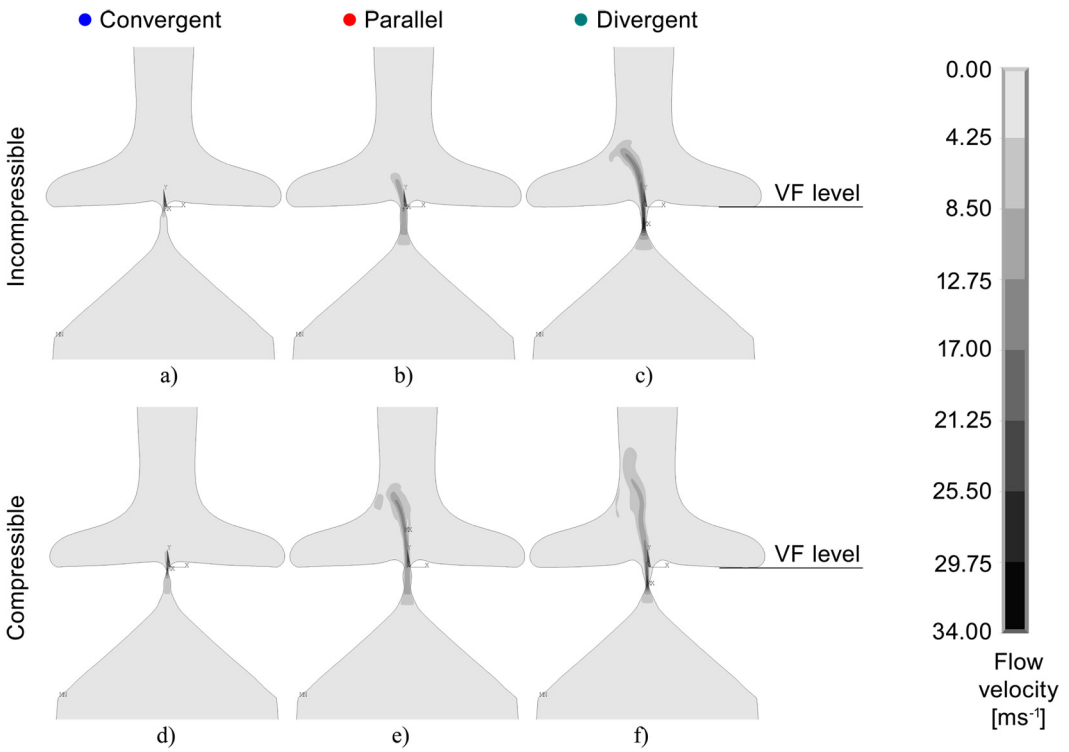

Fig. 5. Flow velocity in the glottis in incompressible (top panels a–c) and compressible (bottom panels d–f) air models. Three time instants are selected displaying a), d) convergent; b), e) parallel, and c), f) divergent glottal shapes. The VF upper surface level is related to the line marked in Fig. 6

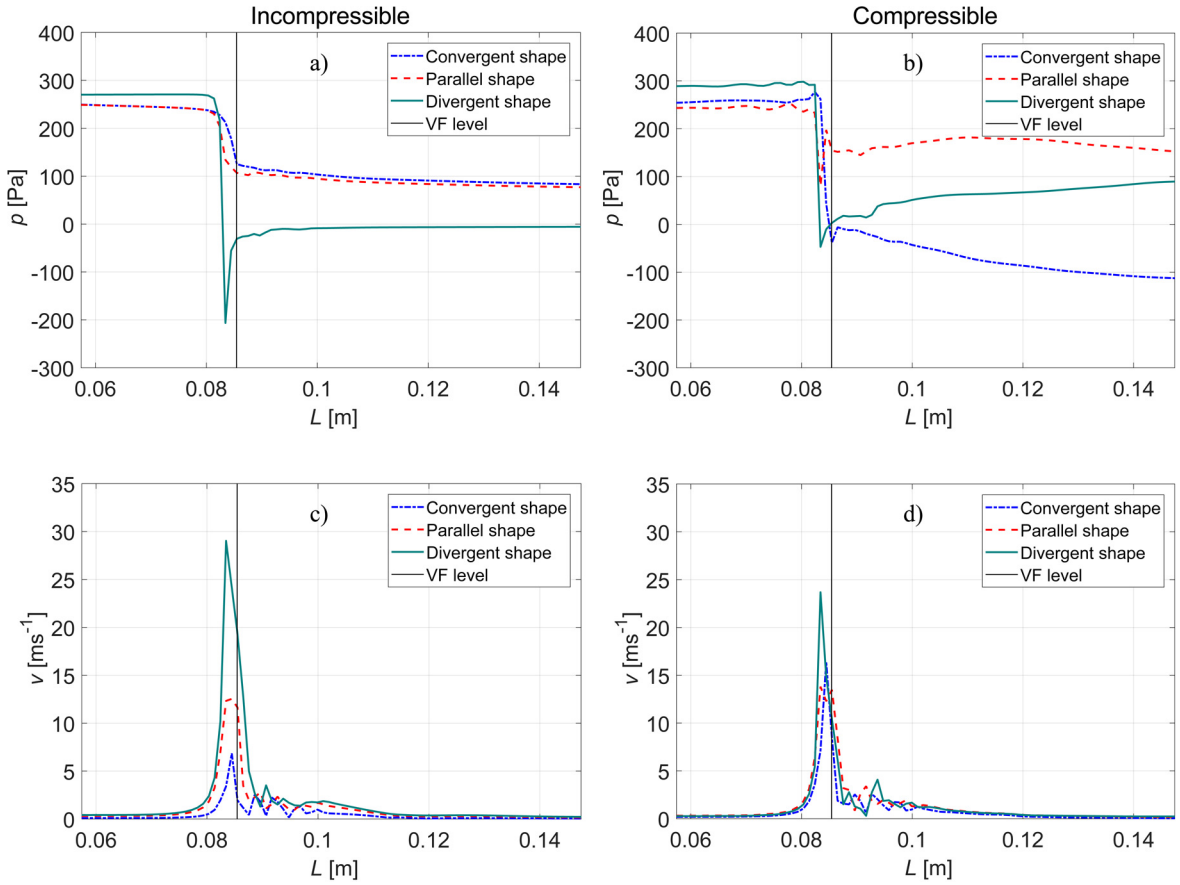

Fig. 6. Comparison of the centerline axis air pressures (panels a, b) and flow velocities (panels c, d) for incompressible (left) and compressible flow (right). The style and color of the lines correspond to convergent, parallel and divergent glottal shapes as marked in Fig. 4. The VF upper surface level is marked by the thin black line

The pressures and flow velocities along the airways axis are depicted in Fig. 6 for the same time instants as in Figs. 4 and 5. The analyzed region was chosen similar to [4].

The changing shape of the VFs during the oscillatory cycle influences the pressure and velocity distribution along the FE model from the trachea to the epilarynx. The pressures shown in Figs. 6a and 6b evince similar dependence: in the trachea, the pressure is close to the preset value of 270 Pa and it drops after passing the VFs. The largest pressure drop occurs during the divergent shape independently of compressibility which corresponds to the observations in [4, 19, 45, 63]. A local minimum of the pressure during the divergent glottis appears just below the upper surface of the VFs. The higher pressure below VFs and the lower above the VFs ensure nonzero airflow, which allows the VF oscillation [4].

The centerline velocities for the incompressible and compressible airflows are shown in Figs. 6c and 6d, respectively. As expected, the highest velocities occur just below the upper VF level in the narrowest part of the glottal channel. The overall shape of the velocity curves is similar for the both computed variants, as is the location of the highest velocity peak during the divergent shape. The location of the velocity peak in the divergent glottal shape matches the local minima of the centerline pressure; the match between the pressure minimum and velocity maximum is a logical consequence of the energy preservation principle and agrees with the data reported in [4, 45]. A deeper pressure drop produces higher peak in the centerline velocity.

When the flow passes the VF level, there is a region influenced by vortices in the expanded duct closely above the VF level. Except for the glottis and surrounding areas where the flow velocities can exceed $20\ \mathrm{m} \cdot \mathrm{s}^{-1}$, the velocities are low, around $1\ \mathrm{m} \cdot \mathrm{s}^{-1}$.

4. Overall discussion and conclusion

This study presents a 2D FE model which simulates airflow-driven self-sustained oscillations of the VFs with collisions, interacting with subglottal and VT, solved numerically using compressible Navier-Stokes equations. The model inherently incorporates the complete fluid-structure-acoustic interactions. To the best of our knowledge, such level of complexity for the modeling of phonatory phenomena has not yet been reported in the literature.

In this study, the model was explored to study the influence of air compressibility on the resulting flow, vibratory and acoustic parameters while keeping all other model parameters constant. In FE modeling studies, the air in the trachea and the VT is commonly considered to be incompressible. This approach simplifies the simulation, but disregards interactions between acoustics and the flow and between acoustics and the VF structure. If we put the acoustic interactions aside, incompressible flow should meet, in general, two conditions: The first one – the flow velocity should be low, under $\mathrm{Ma} = 0.3$ (c. $106\ \mathrm{m} \cdot \mathrm{s}^{-1}$) [6]. In our study, the maximal flow velocities v_g, which appeared in the glottal region, were under $35\ \mathrm{m} \cdot \mathrm{s}^{-1}$ (c. $\mathrm{Ma} = 0.1$). These are rather low velocities which meet the condition. They can be related to the rather low lung pressure p_L. The values of the v_g and p_L can be expected to be two to four times higher in simulations related to the most common conditions from healthy human phonations [4, 38–40, 61, 72], which still meets the condition on low Mach number. And the second one – the variation of the fluid density in the flow should be minimal [82]. Our simulations with compressible equations reveal that the obtained density variation is nearly thousand times smaller than the mean value of air density. Thus the second condition is met also.

Results from our model indicate, however, that the incompressible flow should be used carefully even if these two assumptions are fulfilled. Most importantly, the complete FSAI should be considered for accurate modeling of the phonatory phenomena to include generally non-linear relationships between acoustics and other two fields.

Two types of non-linear source-tract interactions can be distinguished in a phonatory system [75, 77]: level 1 interactions, where the glottal flow waveform is influenced by acoustic resonances; and level 2 interactions, where the acoustic resonances influence also the VF oscillations. Our simulations with compressible air demonstrate the influence of VT acoustics on both the glottal flow (Fig. 4) and on the VF oscillations (Fig. 3).

The air compressibility affects the VF motion, glottal flow, and the pressure waves in the VT. The most affected quantity was the open quotient OQ, while the vibration frequency f_0 was affected much less. Both the incompressible and compressible models achieved symmetric and stabilized self-oscillations after a few periods of a transient regime. The VFs changed their shape between convergent and divergent, and the fundamental vibration frequency f_0 matched that of the human VFs [72].

As far as the limitations are concerned, the model presented here had numerical difficulties with the glottal fluid mesh, which was heavily distorted in cases of increased lung pressure values. Therefore the lung pressure was kept rather low here. This limitation is planned to be addressed in future studies.

For simplicity, VT for only one Czech vowel, [iː], was considered here. The formant frequencies of the simulated vowel were in good agreement with the vowel formant frequencies observed

in Czech speakers [56], with the results of other experiments based on VT with the identical geometry [32] and with the formant frequencies from the sound signal measured during the MRI scan [80].

In principle, the model allows using any VT shapes for different vowels. This opens up new possibilities for investigating the phonatory phenomena relevant for human phonation including the influence of different VT shapes on the VF oscillations. Information on these phenomena is relevant not only for understanding the physiologic speech processes, but also for speech therapy and singing voice where the source-vocal tract interactions are considered to play an important role [30, 49, 74, 76, 81].

Acknowledgements

This work was supported by Czech Science Foundation project No. 19-04477S "Modelling and measurements of fluid-structure-acoustic interactions in biomechanics of human voice production". Access to computing and storage facilities owned by parties and projects contributing to the National Grid Infrastructure MetaCentrum provided under the programme "Projects of Large Research, Development, and Innovations Infrastructures" (CESNET LM2015042), is greatly appreciated.

References

[1] Alipour, F., Scherer, R. C., Vocal fold bulging effects on phonation using a biophysical computer model, Journal of Voice 14 (4) (2000) 470–483. https://doi.org/10.1016/S0892-1997(00)80004-1

[2] Alipour-Haghighi, F., Berry, D. A., Titze, I. R., A finite-element model of vocal-fold vibration, Journal of the Acoustical Society of America 108 (6) (2000) 3003–3012. https://doi.org/10.1121/1.1324678

[3] Alipour-Haghighi, F., Fan, C., Scherer, R. C., A numerical simulation of laryngeal flow in a forced-oscillation glottal model, National Center for Voice and Speech Status and Progress Report 10 (1996) 35–44. https://doi.org/10.1006/csla.1996.0005

[4] Alipour-Haghighi, F., Scherer, R. C., Time-dependent pressure and flow behavior of a self-oscillating laryngeal model with ventricular folds, Journal of Voice 29 (6) (2015) 649–659. https://doi.org/10.1016/j.jvoice.2014.10.021

[5] ANSYS®, Academic research mechanical, Release 9.0, Theory guide, ANSYS, Inc., 2004.

[6] ANSYS®, Academic research mechanical, Release 15.0, Theory guide, ANSYS, Inc., 2013.

[7] Arnela, M., Guasch, O., Finite element synthesis of diphthongs using tuned two-dimensional vocal tracts, IEEE/ACM Transactions on Audio, Speech, and Language Processing 25 (10) (2017) 2013–2023. https://doi.org/10.1109/TASLP.2017.2735179

[8] Axisa, F., Antunes, J., Modelling of mechanical systems: Fluid-structure interaction, 1st edition, Elsevier, Academic Press, 2007. https://doi.org/10.1016/S1874-7051(07)80003-X

[9] Bae, Y., Moon, Y. J., Computation of phonation aeroacoustics by an INS/PCE splitting method, Computers & Fluids 37 (10) (2008) 1332–1343. https://doi.org/10.1016/j.compfluid.2007.12.002

[10] Baken, D. J., Orlikoff, R. F., Clinical measurement of speech and voice, 2nd edition, San Diego, Singular, 2000.

[11] Balázsová, M., Feistauer, M., Horáček, J., Hadrava, M., Kosík, A., Space-time discontinuous Galerkin method for the solution of fluid-structure interaction, Applications of Mathematics 63 (6) (2018) 739–764. https://doi.org/10.21136/AM.2018.0139-18

[12] Barrichelo, V. M., Heuer, R. J., Dean, C. M., Sataloff, R. T., Comparison of singer's formant, speaker's ring, and LTA spectrum among classical singers and untrained normal speakers, Journal of Voice 15 (3) (2001) 344–350. https://doi.org/10.1016/S0892-1997(01)00036-4

[13] Bathe, K. J., Ledezma, G. A., Benchmark problems for incompressible fluid flows with structural interactions, Computers and Structures 85 (11–14) (2007) 628–644. https://doi.org/10.1016/j.compstruc.2007.01.025

[14] van den Berg, J., Myoelastic-aerodynamic theory of voice production, Journal of Speech, Language, and Hearing Research 1 (3) (1958) 227–244. https://doi.org/10.1044/jshr.0103.227

[15] Chan, R. W., Titze, I. R., Viscoelastic shear properties of human vocal fold mucosa: Measurement methodology and empirical results, The Journal of the Acoustical Society of America 106 (4) (1999) 2008–2021. https://doi.org/10.1121/1.427947

[16] Childers, D. G., Lee, C. K., Vocal quality factors: Analysis, synthesis, and perception, The Journal of the Acoustical Society of America 90 (5) (1991) 2394–2410. https://doi.org/10.1121/1.402044

[17] Crighton, D. G., Computational aeroacoustics for low Mach number flows, In: Computational aeroacoustics, (editors) Hardin, J. C., Hussaini, M. Y., New York, Springer New York, 1993, pp. 50–68. https://doi.org/10.1007/978-1-4613-8342-0_3

[18] Curle, N., Lighthill, M. J., The influence of solid boundaries upon aerodynamic sound, Proceedings of the Royal Society of London, Series A, Mathematical and Physical Sciences 231 (1187) (1955) 505–514. https://doi.org/10.1098/rspa.1955.0191

[19] de Oliveira Rosa, M., Pereira, J. C., Grellet, M., Alwan, A., A contribution to simulating a three-dimensional larynx model using the finite element method, The Journal of the Acoustical Society of America 114 (5) (2003) 2893–2905. https://doi.org/10.1121/1.1619981

[20] Dedouch, K., Horáček, J., Vampola, T., Švec, J. G., Kršek, P., Havlík, R., Acoustic modal analysis of male vocal tract for Czech vowels, Proceedings of Interaction and Feedback 2002, Prague, Institute of Thermomechanics of the Czech Academy of Sciences, 2002, pp. 13–20.

[21] Degroote, J., Bathe, K. J., Vierendeels, J., Performance of a new partitioned procedure versus a monolithic procedure in fluid-structure interaction, Computers and Structures 87 (11–12) (2009) 793–801. https://doi.org/10.1016/j.compstruc.2008.11.013

[22] Ewert, R., Schröder, W., Acoustic perturbation equations based on flow decomposition via source filtering, Journal of Computational Physics 188 (2) (2003) 365–398. https://doi.org/10.1016/S0021-9991(03)00168-2

[23] Ewins, D. J., Rao, S. S., Braun, S., Encyclopedia of vibration, 1st edition, London, Academic Press, 2002.

[24] Falk, S., Kniesburges, S., Schoder, S., Jakubaß, B., Maurerlehner, P., Echternach, M., Kaltenbacher, M., Döllinger, M., 3D-FV-FE aeroacoustic larynx model for investigation of functional based voice disorders, Frontiers in Physiology 12 (2021) 1–17. https://doi.org/10.3389/fphys.2021.616985

[25] Ffowcs Williams, J. E., Hawkings, D. L., Sound generation by turbulence and surfaces in arbitrary motion, Philosophical Transactions of the Royal Society of London. Series A, Mathematical and Physical Sciences 264 (1151) (1969) 321–342. https://doi.org/10.1098/rsta.1969.0031

[26] Flanagan, J. L., Landgraf, L. L., Self-oscillating source for vocal-tract synthesizers, IEEE Transactions on Audio and Electroacoustics 16 (1) (1968) 57–64. https://doi.org/10.1109/TAU.1968.1161949

[27] Fulcher, L. P., Scherer, R. C., De Witt, K. J., Thapa, P., Bo, Y., Kucinschi, B. R., Pressure distributions in a static physical model of the hemilarynx: Measurements and computations, Journal of Voice 24 (1) (2010) 2–20. https://doi.org/10.1016/j.jvoice.2008.02.005

[28] Hájek, P., Švancara, P., Horáček, J., Švec, J. G., Finite element modelling of the effect of stiffness and damping of vocal fold layers on their vibrations and produced sound, Applied Mechanics and Materials 821 (2016) 657–664. https://doi.org/10.4028/www.scientific.net/AMM.821.657

[29] Hájek, P., Švancara, P., Horáček, J., Švec, J. G., Effects of turbulence in FE model of human vocal folds self-oscillation, Proceedings of the conference Engineering Mechanics 2017, Svratka, Czech Republic, pp. 366–369.

[30] Henrich, N., Smith, J., Wolfe, J., Vocal tract resonances in singing: Strategies used by sopranos, altos, tenors, and baritones, The Journal of the Acoustical Society of America 129 (2) (2011) 1024–1035. https://doi.org/10.1121/1.3518766

[31] Horáček, J., Švec, J. G., Aeroelastic model of vocal-fold-shaped vibrating element for studying the phonation treshold, Journal of Fluids and Structures 16 (7) (2002) 931–955. https://doi.org/10.1006/jfls.2002.0454

[32] Horáček, J., Uruba, V., Radolf, V., Veselý, J., Bula, V., Airflow visualization in a model of human glottis near the self-oscillating vocal folds model, Applied and Computational Mechanics 5 (1) (2011) 21–28.

[33] Ishizaka, K., Flanagan, J. L., Synthesis of voiced sounds from a two-mass model of the vocal cords, Bell System Technical Journal 51 (6) (1972) 1233–1268. https://doi.org/10.1002/j.1538-7305.1972.tb02651.x

[34] Jo, Y., Ra, H., Moon, Y. J., Döllinger, M., Three-dimensional computation of flow and sound for human hemilarynx, Computers & Fluids 134–135 (2016) 41–50. https://doi.org/10.1016/j.compfluid.2016.04.029

[35] Kakita, Y., Hirano, M., Ohmaru, K., Physical properties of the vocal fold tissue, Vocal Fold Physiology (1981).

[36] Kaltenbacher, M., Marburg, S., Beck, A., Munz, C. D., Langer, U., Neumüller, M., Computational acoustics, 1st edition, Springer International Publishing, 2018.

[37] Kaneko, T., Uchida, K., Komatsu, K., Kanesaka, T., Kobayashi, N., Naito, J., Mechancial properties of the vocal fold: Measurement in-vivo, In: Vocal fold physiology, Tokyo University, Tokyo, 1981, pp. 365–376.

[38] Khosla, S., Muruguppan, S., Gutmark, E., Scherer, R. C., Vortical flow field during phonation in an excised canine larynx model, Annals of Otology, Rhinology and Laryngology 116 (3) (2007) 217–228. https://doi.org/10.1177/000348940711600310

[39] Khosla, S., Oren, L., Ying, J., Gutmark, E., Direct simultaneous measurement of intraglottal geometry and velocity fields in excised larynges, The Laryngoscope 124 (S2) (2014) S1–S13. https://doi.org/10.1002/lary.24512

[40] Krane, M., Barry, M., Wei, T., Unsteady behavior of flow in a scaled-up vocal folds model, The Journal of the Acoustical Society of America 122 (6) (2007) 3659–3670. https://doi.org/10.1121/1.2409485

[41] Lighthill, M. J., On sound generated aerodynamically II. Turbulence as a source of sound, Proceedings of the Royal Society of London. Series A. Mathematical and Physical Sciences 222 (1148) (1954) 1–32. https://doi.org/10.1098/rspa.1954.0049

[42] Lighthill, M. J., Newman, A. M. H., On sound generated aerodynamically I. General theory, Proceedings of the Royal Society of London. Series A. Mathematical and Physical Sciences 211 (1107) (1952) 564–587. https://doi.org/10.1098/rspa.1952.0060

[43] Link, G., Kaltenbacher, M., Breuer, M., Döllinger, M., A 2D finite-element scheme for fluid–solid–acoustic interactions and its application to human phonation, Computer Methods in Applied Mechanics and Engineering 198 (41) (2009) 3321–3334. https://doi.org/10.1016/j.cma.2009.06.009

[44] Lohscheller, J., Švec, J. G., Döllinger, M., Vocal fold vibration amplitude, open quotient, speed quotient and their variability along glottal length: Kymographic data from normal subjects, Logopedics Phoniatrics Vocology 38 (4) (2013) 182–192. https://doi.org/10.3109/14015439.2012.731083

[45] Mihaescu, M., Khosla, S. M., Murugappan, S., Gutmark, E. J., Unsteady laryngeal airflow simulations of the intra-glottal vortical structures, The Journal of the Acoustical Society of America 127 (1) (2010) 435–444. https://doi.org/10.1121/1.3271276

[46] Murtola, T., Aalto, A., Malinen, J., Aalto, D., Vainio, M., Modal locking between vocal fold oscillations and vocal tract acoustics, Acta Acustica united with Acustica 104 (2018) 323–337. https://doi.org/10.3813/AAA.919175

[47] Pelorson, X., Hirschberg, A., van Hassel, R. R., Wijnands, A. P. J., Auregan, Y., Theoretical and experimental study of quasisteady-flow separation within the glottis during phonation – Application to a modified two-mass model, The Journal of the Acoustical Society of America 96 (6) (1994) 3416–3431. https://doi.org/10.1121/1.411449

[48] Rosenberg, A. E., Effect of glottal pulse shape on the quality of natural vowels, The Journal of the Acoustical Society of America 49 (2B) (1971) 583–590. https://doi.org/10.1121/1.1912389

[49] Rothenberg, M., Source-tract acoustic interaction in the soprano voice and implications for vocal efficiency, In: Vocal fold physiology, College Hill Press, San Diego, 1986, pp. 254–263.

[50] Sadeghi, H., Kniesburges, S., Falk, S., Kaltenbacher, M., Schützenberger, A., Döllinger, M., Towards a clinically applicable computational larynx model, Applied Sciences 9 (11) (2019) 2288. https://doi.org/10.3390/app9112288

[51] Sadeghi, H., Kniesburges, S., Kaltenbacher, M., Schützenberger, A., Döllinger, M., Computational models of laryngeal aerodynamics: Potentials and numerical costs, Journal of Voice 33 (4) (2019) 385–400. https://doi.org/10.1016/j.jvoice.2018.01.001

[52] Scherer, R. C., Shinwari, D., De Witt, K. J., Zhang, C., Kucinschi, B. R., Afjeh, A. A., Intraglottal pressure profiles for a symmetric and oblique glottis with a divergence angle of 10 degrees, The Journal of the Acoustical Society of America 109 (4) (2001) 1616–1630. https://doi.org/10.1121/1.1333420

[53] Schickhofer, L., Malinen, J., Mihaescu, M., Compressible flow simulations of voiced speech using rigid vocal tract geometries acquired by MRI, The Journal of the Acoustical Society of America 145 (4) (2019) 2049–2061. https://doi.org/10.1121/1.5095250

[54] Schickhofer, L., Mihaescu, M., Analysis of the aerodynamic sound of speech through static vocal tract models of various glottal shapes, Journal of Biomechanics 99 (2020) 109484. https://doi.org/10.1016/j.jbiomech.2019.109484

[55] Sigrist, J. F., Fluid-structure interaction: An introduction to finite element coupling, Chicheste, Wiley & Sons, 2015. https://doi.org/10.1002/9781118927762

[56] Skarnitzl, R., Volín, J., Reference values of vowel formants for young adult speakers of standard Czech, Akustické listy 18 (1) (2012) 7–11. (in Czech)

[57] Story, B. H., Titze, I. R., Voice simulation with a body-cover model of the vocal folds, The Journal of the Acoustical Society of America 97 (2) (1995) 1249–1260. https://doi.org/10.1121/1.412234

[58] Suh, J., Frankel, S. H., Numerical simulation of turbulence transition and sound radiation for flow through a rigid glottal model, The Journal of the Acoustical Society of America 121 (6) (2007) 3728–3739. https://doi.org/10.1121/1.2723646

[59] Sundberg, J., The acoustics of the singing voice, Scientific American Magazine (1977) 82–91. https://doi.org/10.1038/scientificamerican0377-82

[60] Sváček, P., Horáček, J., Finite element approximation of flow induced vibrations of human vocal folds model: Effects of inflow boundary conditions and the length of subglottal and supraglottal channel on phonation onset, Applied Mathematics and Computation 319 (2018) 178–194. https://doi.org/10.1016/j.amc.2017.02.026

[61] Šidlof, P., Doaré, O., Cadot, O., Chaigne, A., Measurement of flow separation in a human vocal folds model, Experiments in Fluids 51 (1) (2011) 123–136. https://doi.org/10.1007/s00348-010-1031-9

[62] Šidlof, P., Horáček, J., Řidký, V., Parallel CFD simulation of flow in a 3D model of vibrating human vocal folds, Computers & Fluids 80 (2013) 290–300. https://doi.org/10.1016/j.compfluid.2012.02.005

[63] Šidlof, P., Zörner, S., Hüppe, A., A hybrid approach to the computational aeroacoustics of human voice production, Biomechanics and Modeling in Mechanobiology 14 (3) (2014) 473–488. https://doi.org/10.1007/s10237-014-0617-1

[64] Švancara, P., Horáček, J., Hrůza, V., FE modelling of the fluid-structure-acoustic interaction for the vocal folds self-oscillation, Vibration Problems ICOVP 2011 SE – 108, Springer Proceedings in Physics, vol. 139, 2011, pp. 801–807. https://doi.org/10.1007/978-94-007-2069-5_108

[65] Švancara, P., Horáček, J., Švec, J. G., Numerical simulation of the self-oscillations of the vocal folds and of the resulting acoustic phenomena in the vocal tract, Advances in Mechanisms Design SE–47, Mechanisms and Machine Science, vol. 8, 2012, pp. 357–363. https://doi.org/10.1007/978-94-007-5125-5_47

[66] Švec, J. G., Schutte, H. K., Chen, C. J., Titze, I. R., Integrative insights into the myoelastic-aerodynamic theory and acoustics of phonation – Scientific tribute to Donald G. Miller, Journal of Voice (2021). https://doi.org/10.1016/j.jvoice.2021.01.023

[67] Tanabe, M., Isshiki, N., Sawada, M., Damping ratio of the vocal cord, Folia Phoniatrica et Logopaedica 31 (1) (1979) 27–34. https://doi.org/10.1159/000264147

[68] Tao, C., Jiang, J. J., Zhang, Y., Simulation of vocal fold impact pressures with a self-oscillating finite-element model, The Journal of the Acoustical Society of America 119 (6) (2006) 3987–3994. https://doi.org/10.1121/1.2197798

[69] Thomson, S. L., Mongeau, L., Frankel, S. H., Aerodynamic transfer of energy to the vocal folds, Journal of the Acoustical Society of America 118 (3) (2005) 1689–1700. https://doi.org/10.1121/1.2000787

[70] Titze, I. R., Comments on the myoelastic-aerodynamic theory of phonation, Journal of Speech, Language, and Hearing Research 23 (3) (1980) 495–510. https://doi.org/10.1044/jshr.2303.495

[71] Titze, I. R., The physics of small-amplitude oscillation of the vocal folds, The Journal of the Acoustical Society of America 83 (4) (1988) 1536–1552. https://doi.org/10.1121/1.395910

[72] Titze, I. R., Principles of voice production, Englewood Cliffs, New Yersey, Prentice-Hall, Inc., 1994.

[73] Titze, I. R., The myoelastic aerodynamic theory of phonation, Denver and Iowa City, National Centre for Voice and Speech, 2006.

[74] Titze, I. R., Voice training and therapy with a semi-occluded vocal tract: Rationale and scientific underpinnings, Journal of Speech, Language, and Hearing Research 49 (2) (2006) 448–459. https://doi.org/10.1044/1092-4388(2006/035)

[75] Titze, I. R., Nonlinear source–filter coupling in phonation: Theory, Journal of the Acoustical Society of America 123 (5) (2008) 2733–2749. https://doi.org/10.1121/1.2832337

[76] Titze, I. R., The human instrument, Scientific American 298 (1) (2008) 94–101. https://doi.org/10.1038/scientificamerican0108-94

[77] Titze, I. R., Riede, T., Popolo, P., Nonlinear source–filter coupling in phonation: Vocal exercises, The Journal of the Acoustical Society of America 123 (4) (2008) 1902–1915. https://doi.org/10.1121/1.2832339

[78] Tokuda, I., Zemke, M., Kob, M., Herzel, H., Biomechanical modeling of register transitions and the role of vocal tract resonators, The Journal of the Acoustical Society of America 127 (3) (2010). https://doi.org/10.1121/1.3299201

[79] Tokuda, I. T., Horáček, J., Švec, J. G., Herzel, H., Comparison of biomechanical modeling of register transitions and voice instabilities with excised larynx experiments, The Journal of the Acoustical Society of America 122 (1) (2007) 519–531. https://doi.org/10.1121/1.2741210

[80] Vampola, T., Horáček, J., Švec, J. G., FE modeling of human vocal tract acoustics – Part I: Production of Czech vowels, Acta Acustica united with Acustica 94 (3) (2008) 433–447. https://doi.org/10.3813/AAA.918051

[81] Vampola, T., Laukkanen, A. M., Horáček, J., Švec, J. G., Vocal tract changes caused by phonation into a tube: A case study using computer tomography and finite-element modeling, The Journal of the Acoustical Society of America 129 (1) (2011) 310–315. https://doi.org/10.1121/1.3506347

[82] Versteeg, H. K., Malalasekera, W., An introduction to computational fluid dynamics: The finite volume method, 2nd edition, Harlow, Pearson Education Limited, 2007.

[83] Xue, Q., Zheng, X., Mittal, R., Bielamowicz, S., Subject-specific computational modeling of human phonation, The Journal of the Acoustical Society of America 135 (3) (2014) 1445–1456. https://doi.org/10.1121/1.4864479

[84] Zhang, C., Zhao, W., Frankel, S. H., Mongeau, L., Computational aeroacoustics of phonation, Part II: Effects of flow parameters and ventricular folds, The Journal of the Acoustical Society of America 112 (5) (2002) 2147–2154. https://doi.org/10.1121/1.1506694

[85] Zhao, W., Zhang, C., Frankel, S. H., Mongeau, L., Computational aeroacoustics of phonation, Part I: Computational methods and sound generation mechanisms, The Journal of the Acoustical Society of America 112 (5) (2002) 2134–2146. https://doi.org/10.1121/1.1506693

[86] Zheng, X., Mittal, R., Xue, Q., Bielamowicz, S., Direct-numerical simulation of the glottal jet and vocal-fold dynamics in a three-dimensional laryngeal model, The Journal of the Acoustical Society of America 130 (1) (2011) 404–415. https://doi.org/10.1121/1.3592216

[87] Zörner, S., Kaltenbacher, M., Döllinger, M., Investigation of prescribed movement in fluid–structure interaction simulation for the human phonation process, Computers & Fluids 86 (2013) 133–140. https://doi.org/10.1016/j.compfluid.2013.06.031